Available online at www.sciencedirect.com

SciVerse ScienceDirect

Ceramics International 39 (2013) 2175–2181

CERAMICS INTERNATIONAL

www.elsevier.com/locate/ceramint

Short communication

Carbon-filament-entangled lithium iron phosphate/carbon composite produced in partially reductive atmosphere: Dual role of the iron as source material and catalyst

Jinhan Yao[a,*], Jianbo Wang[a], Pinjie Zhang[a], Duncan H. Gregory[b], Chun'an Ma[a], Lianbang Wang[a,*]

[a]*State Key Laboratory Breeding Base of Green Chemistry-Synthesis Technology, College of Chemical Engineering and Material Science, Zhejiang University of Technology, Hangzhou, Zhejiang, PR China*

[b]*WestCHEM, School of Chemistry, University of Glasgow, Glasgow G12 8QQ, UK*

Received 1 August 2012; received in revised form 2 August 2012; accepted 2 August 2012
Available online 9 August 2012

Abstract

Various morphologies of carbon-$LiFePO_4$ composites can be achieved *via* the reaction of the appropriate iron or iron oxalate and hydrated phosphates with sucrose as the source of carbon in the Ar/H_2 or Ar atmosphere. When sintering in Ar condition, the resulting composite comprised a $LiFePO_4$ core coated with a carbon shell. By contrast, Ar/H_2-derived composites produced under a partially reductive atmosphere consisted of olivine particles enmeshed in a carbon filament matrix with the catalytic effect of Fe. Specific capacities as high as 140 mA h g^{-1} at 1 C and 93 mA h g^{-1} at 10 C were obtained in carbon-filament-entangled $LiFePO_4$ composite.

Keywords: Solid state reaction; Iron; Sintering atmosphere

1. Introduction

Olivine-type $LiFePO_4$, a promising cathode material to replace the current state of the art material, $LiCoO_2$, has a high theoretical capacity of 170 mA h g^{-1} and a redox potential of 3.45 V versus Li/Li^+. Several synthetic routes have been developed for the preparation of lithium ion cathode materials. These include solid-state reactions [1–4], hydrothermal procedures [5,6], sol–gel methods [7,8], microwave synthesis [9,10] and co-precipitation [11]. Among these methods, the solid-state reaction route [12] is regarded as one of the most practical ways to scale-up. However, finding a low-cost synthetic route to yield high performance $LiFePO_4$ products remains a challenge. In this regard, the selection of cheap Fe and $FePO_4$ over divalent ferrous source such as FeC_2O_4 would greatly reduce production cost.

One of key issues to overcome in $LiFePO_4$ is the low electronic conductivity (10^{-9}–10^{-10} S cm^{-1}). At the origin of this is the strong P–O covalent bond that causes the separation of FeO_6 octahedrons in the structure where electrons cannot transport through the Fe–O–Fe bond [13,14]. Since the original work of Padhi et al [15], $LiFePO_4$ has been the subject of intensive research to (1) develop an efficient synthetic route; (2) modify the materials (at the surface and in the bulk) to increase electronic and Li^+ ionic conductivity.

Further synthetic procedures have been investigated to address the issue of surface reactivity and conductivity. A successful surface treatment could protect the surface and/or alter/improve some of the key traits of electrode materials, e.g. suppressing the electrode/electrolyte by-reaction [16] or increasing the electronic conductivities [17]. Carbon surface coating is yet another widely-proven measure in enhancing the electronic conductivity of $LiFePO_4$. Various carbon sources have been used to prepare $LiFePO_4$/C composites [11–17]. In fact, with a deeper understanding of the role of carbon modification, it

*Corresponding author. Tel.: +86 571 88320611; fax: +86 571 88320832.
E-mail addresses: jhyao@zjut.edu.cn (J. Yao), Wanglb99@zjut.edu.cn (L. Wang).

0272-8842/$ - see front matter © 2012 Elsevier Ltd and Techna Group S.r.l. All rights reserved.
http://dx.doi.org/10.1016/j.ceramint.2012.08.001

was found that optimizing electrochemical properties of $LiFePO_4$/C composites strongly depends on the nature of the carbon coating or composite, e.g. homogeneity and morphology [1,18]. In particular, Pan et al. [19] recently pointed out that carbon coatings with different pore structures, have different influences on the electrochemical properties of resultant $LiFePO_4$/C composites. This indicates that the morphology of the carbon coating layer (in turn dependent on synthesis parameters such as temperature and atmosphere) in the $LiFePO_4$/C composites is a key issue that should not be ignored.

We report here a mechano-chemical-solid-state synthesis method using Li_3PO_4 as Li source combined with Fe and $FePO_4$ as widely available Fe sources. We discuss the role of Fe under a partially reductive atmosphere on the physical and electrochemical properties of the resultant $LiFePO_4$/C composites. We discovered that by using Ar/H_2 as a protection atmosphere, a carbon-filament-network was in situ formed in the $LiFePO_4$/C composite, possibly with catalytic effect of Fe. By contrast, composites derived from Ar atmosphere or exclusion of Fe as source material showed that carbon layers form on the surface of $LiFePO_4$ particles. The Ar/H_2-derived carbon filament entangled $LiFePO_4$/C composites demonstrated enhanced cyclabilities and high rate capabilities illustrating that the microstructure of the composite is vital in engineering electrochemical performance in olivine-based cathodes.

2. Experimental

2.1. Chemicals and synthesis of $LiFePO_4$/C composites

The $LiFePO_4$/C composite was synthesized *via* the solid-state reaction of $FePO_4 \cdot 4H_2O$, Fe, $Li_3PO_4 \cdot 0.5H_2O$ (Sinopharm Chemical Reagent Co., Ltd.) and sucrose (Guangdong Guanghua Chemcial Factory Co., Ltd.) as a source of carbon. All of the chemicals were analytical reagents except for $FePO_4 \cdot 4H_2O$ and $Li_3PO_4 \cdot 0.5H_2O$. The mixtures containing 15.0 wt% sucrose were ball-milled (planetary type, agate ball, ball diameter of 10 mm) in an agate jar using a rotating speed of ca. 200 rpm for 5 h. After the ethanol was removed, the precursor mixture was heated at 723 K for 6 h and then 1073 K for 10 h under a Ar(95%)–H_2(5%), Ar atmosphere respectively. The samples were allowed to cool naturally to room temperature and designated AH-$LiFePO_4$, A-$LiFePO_4$. To verify the effect of Fe during the synthesis, a parallel preparation was conducted using FeC_2O_4 (not Fe) as Fe source also sintering in the Ar(95%)–H_2(5%) atmosphere. The sample was labeled as N-$LiFePO_4$.

2.2. Materials characterization

The crystalline phases of the samples were identified by powder X-ray diffraction (XRD, PANlytical, X'Pert Pro) using Cu Kα radiation (λ=0.154056 nm) in the 2θ range from 10° to 80° with a step-size of 0.03°. Product morphologies were observed by scanning electronic microscopy (SEM, Hitachi S-4700, 15 kV) and transmission electronic microscopy (TEM, Tecnai G2 F30 S-Twin, 300 kV). The carbon content of the $LiFePO_4$/C materials was measured by a Flash EA 1112 tester (Conflo-III, Thermo Electron Corporation, America).The tap density was obtained by the following method: ca. 3 g of the respective $LiFePO_4$/C powders was poured into a small, pre-weighed, calibrated measuring cylinder, which was tapped by hand until the volume of the powder ceased to decrease. The volume, V, was read and the tap density, ρ, thus calculated from $\rho = m/V$ (where m is the mass of the powder). The tap densities of the composite powders are listed in Table 1.

2.3. Electrochemical testing

The electrochemical performance of the as-prepared materials as cathodes was evaluated in a CR2032-type coin cell assembled in an argon filled glove box. The active materials, acetylene black and polyvinylidene fluoride (PVDF) were ground in a 1-methyl-2-pyrrolidinone (NMP) solution in a weight ratio of 8:1:1 to form slurry, which was then pasted onto an aluminum foil current collector and dried at 353 K for 10 h under vacuum. Lithium metal was used as counter electrode. The electrolyte was 1 mol m^{-3} $LiPF_6$ in a solvent mixture of ethylene carbonate (EC), dimethyl carbonate (DMC) and ethylmethyl carbonate (EMC) (1:1:1, $v/v/v$). Charge–discharge tests were performed over a voltage range of 2.5–4.2 V using a Land CT2001A battery test system at 298 K.

Table 1
Summary of structural properties, carbon content and tap densities for the AH-$LiFePO_4$, A-$LiFePO_4$ and N-$LiFePO_4$ samples.

Sample	Preparation			Phase and structure Properties						
	Atmosphere	Phases content		$LiFePO_4$ Lattice constant			*R* value			
		$LiFePO_4$ (%)	Li_3PO_4 (%)	*a* (Å)	*b* (Å)	*c* (Å)	*R* (%)	R_p (%)	Carbon content (%)	Tap densities (g cm^{-3})
AH-$LiFePO_4$	Ar(95%)–H_2	99.40	0.6	10.322(3)	6.008(2)	4.695(2)	2.21	2.32	3.4	1.32
A-$LiFePO_4$	Ar	98.9	1.1	10.321(6)	6.007(8)	4.693(1)	3.31	3.35	3.5	1.30
N-$LiFePO_4$	Ar(95%)–H_2	99.60	0.4	10.325(1)	6.008(7)	4.696(1)	2.54	2.12	3.2	1.33

Cyclic voltammetry (CV) measurements were performed between 2.5–4.2 V with a CHI 660B electrochemical station (Shanghai Chenhua, China) at a scan rate of 0.3 mV s^{-1}.

3. Results and discussion

$LiFePO_4$ can be directly synthesized from Li_3PO_4, $FePO_4$ and Fe (Eq. (1)). The iron powder reduces trivalent Fe(III) in $FePO_4$ into bivalent Fe (II) in the product.

$$Fe + 2FePO_4 + Li_3PO_4 \rightarrow 3LiFePO_4$$

High purity $LiFePO_4$/C composites could be obtained *via* heating the mechanically-milled reactants in the various atmospheres. Fig. 1A shows the X-ray diffraction (XRD) patterns of the resulting AH-$LiFePO_4$, A-$LiFePO_4$ and N-$LiFePO_4$. The observation of sharp, intense peaks indicates highly crystalline samples. With the exception of weak diffraction peaks at $2\theta = 22^\circ$ and 25°, corresponding to Li_3PO_4, all the peaks could be indexed to orthorhombic $LiFePO_4$ (ICPDS card no. 40-1499; space group *Pmnb* (no. 62)). The absence of typical carbon peaks (e.g. at $2\theta = 23^\circ$) indicates that any carbon might be likely amorphous. In addition, carbon is confirmed in Fig. 1B by Raman spectrum. The strong band at 1330 and 1598 cm − 1 are respectively attributed to the D-band (the vibration in opposite direction of neighboring carbon in graphene sheet) and G- band (disorder mode)of carbon [20]. The bands at 200–500 cm^{-1} and 520–1120 cm^{-1} corresponding the Raman vibration absorptions of Fe–O and PO_4^{3-} in $LiFePO_4$ [21]. Olivine phase structures were then refined by using Reflex module of Materials Studio. Table 1 summarizes the phase, structural and related properties for the prepared $LiFePO_4$/C composites. As shown in Table 1, the Li_3PO_4 impurity can be minimized to almost negligible levels. The resultant high purity products can be ascribed to the addition of reductive carbon, which could suppress the formation of relatively high valence Fe (III) impurities such as $Li_3Fe_2(PO_4)_3$ [22]. The lattice constants of $LiFePO_4$ in the three samples were in good agreement with those reported e.g. $a = 10.322$ Å, $b = 6.005$ Å, $c = 4.695$ Å [23]. The carbon content in the samples is 3–4 wt% analyzed by Flash EA 1112 tester. It is worth noting that the tap density of AH-$LiFePO_4$ is higher than those of other two samples due to regular spherical particles and a lower carbon content, which is consistent with the report by Chang et al. [24].

SEM micrographs illustrate the different morphologies of the respective $LiFePO_4$/C composites (Fig. 2). The image in Fig. 2a shows that the A-$LiFePO_4$ sample is composed of particles with a diameter of ca. 1 μm whereas N-$LiFePO_4$ (Fig. 2b) is composed of irregular shaped particles with larger dimensions of ca. 3 μm. Similar irregular shapes and large size distributions of $LiFePO_4$/C composites calcined in the Ar atmosphere were also observed by Cheng et al [25]. According to a previous publication [26], the tap-density of powders is partly related to the shape (symmetry) and size of the particle, in addition to the particle size distribution in the powders. The A-$LiFePO_4$ sample, composed of spherical particles, has a higher density than the N-$LiFePO_4$ sample, composed of irregular particles [18], which is consistent with the tap densities measured in Table 1. By contrast to the A-$LiFePO_4$ and N-$LiFePO_4$ composites, the AH-$LiFePO_4$ is composed not only of spherical particles but also of filament-like carbon materials (Fig. 2c and d), which suggests $LiFePO_4$ particles with a size < 1 μm are embedded in a 3D carbon network. This morphology differs to the carbon coated shell (surface layer) for the A-$LiFePO_4$ and N-$LiFePO_4$ composites.

TEM images (Fig. 3a–d) further confirm that the $LiFePO_4$ particles were entangled within a filament-like carbon matrix. Such a carbon network has the potential to enhance the conductivity and improve the high-power electrochemical performances of $LiFePO_4$ [27]. The carbon network serves as a continuous conductive net embedding $LiFePO_4$ nano-particles to enhance the electron transfer

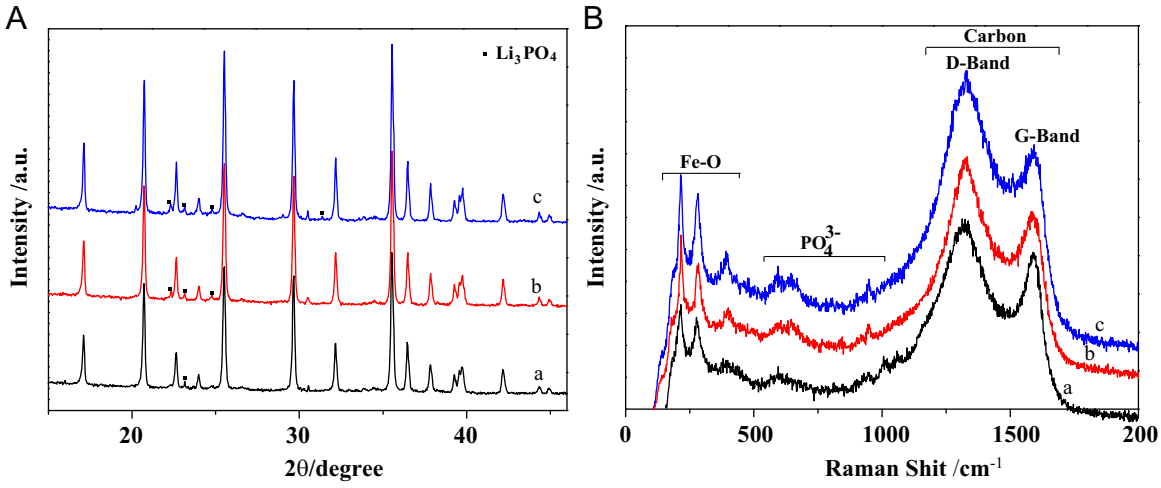

Fig. 1. (A) XRD patterns and (B) Raman spectra of $LiFePO_4$/C composites using sucrose as carbon sources in (a) Ar/H_2, (b) Ar and (c) without Fe in Ar/H_2 atmosphere.

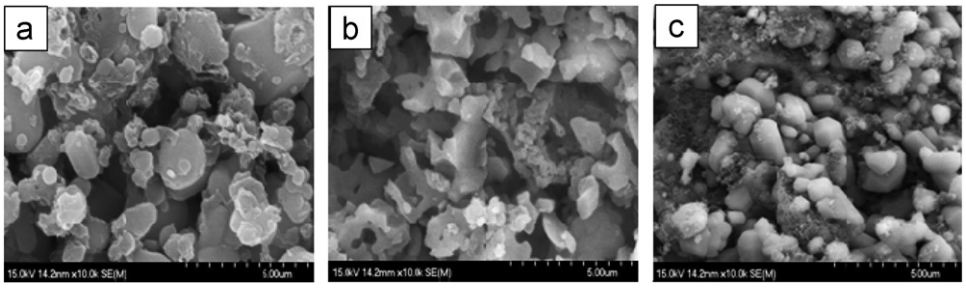

Fig. 2. SEM images of the (a) A-$LiFePO_4$, (b) N-$LiFePO_4$ and (c) AH-$LiFePO_4$ samples.

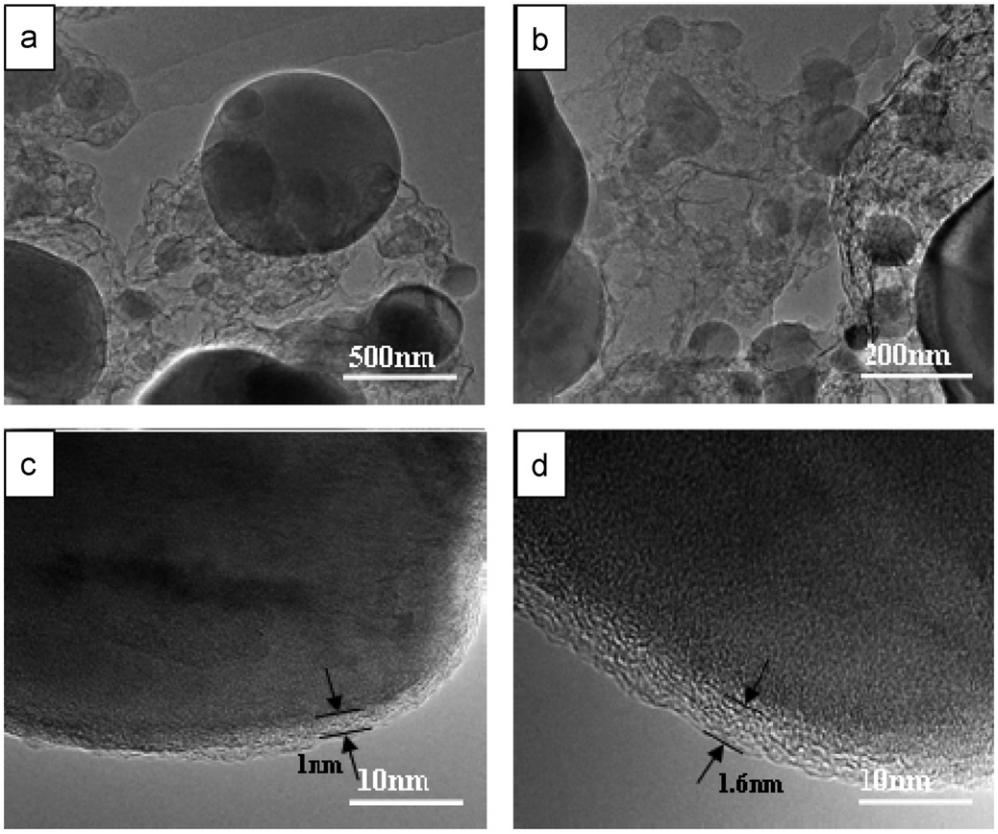

Fig. 3. TEM images of (a,b) AH-$LiFePO_4$/C, (c) A-$LiFePO_4$/C and (d) N-$LiFePO_4$/C.

between $LiFePO_4$ particles [28]. It is also anticipated that the carbon network could act as a robust scaffold for supporting the active material alleviating the volume changes of the $LiFePO_4$–$FePO_4$ two phase transformation and improving the longevity of the cycling performance [29]. The formation of the carbon filaments may be ascribed to the valence compensating effect of H_2 on the formation of carbon via the pyrolysis of sucrose. According to Nolan et al. [30], the formation of open forms of carbon filaments is mainly due to hydrogen compensating for the reduced valence of the coordinatively unsaturated carbon at the free edges of the graphite planes. However, in the case of N-$LiFePO_4$, even with the presence of H_2, carbon was still produced in the "closed" form of carbon particles formed around the particle core. We speculate that the lack of Fe (as catalyst) may be responsible for the inabilities of the formation of carbon filament during the pyrolysis of sucrose. Therefore, both Fe and H_2 would be two necessary factors to generate carbon filament entangled $LiFePO_4$/C composite. Closer observation of an individual AH-$LiFePO_4$ composite particle (Fig. 3d) reveals that a carbon layer also forms around the $LiFePO_4$ particle, suggesting a good contact between the carbon filaments and the core–shell $LiFePO_4$ particles. In a recent report [19], Pan et al. suggested the possibilities of carbon-oxygen bonding (where oxygen originates from $LiFePO_4$) during the solid state formation of $LiFePO_4$/C composites. This C–O bonding at the interface may weaken the ligand

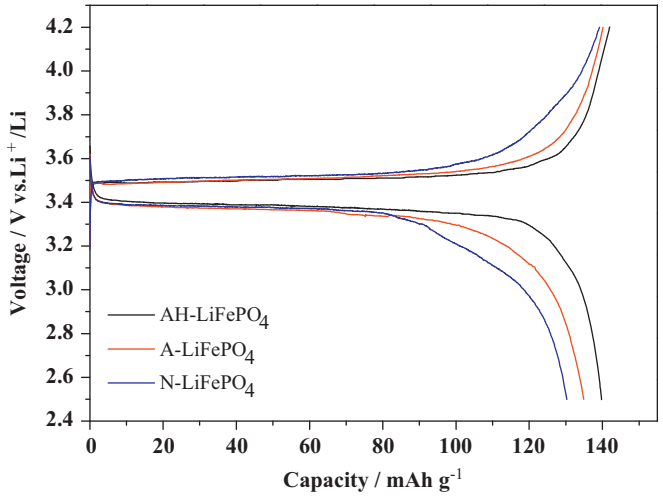

Fig. 4. Initial charge/discharge profiles for AH-$LiFePO_4$, A-$LiFePO_4$ and N-$LiFePO_4$ at a 1 C rate.

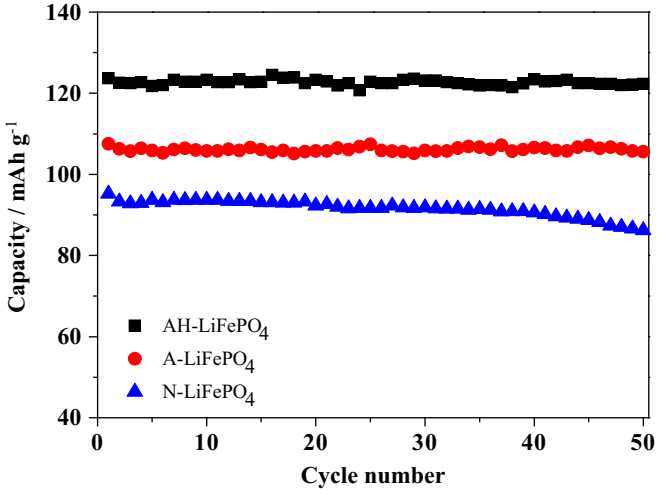

Fig. 5. Comparison of cycling performances of the $LiFePO_4$/C composites at a 2 C rate.

field of the FeO_6 octahedron, leading to a change of spin configuration of ferric ions at the surface [31]. The surface effects on the physical and electrochemical properties for carbon coated $LiFePO_4$ were investigated and it was found that carbon coating of $LiFePO_4$ could switch the Fe^{3+} in the surface layer from low-spin ($S=1/2$) configuration to high-spin ($S=5/2$) configuration. Subsequently the amorphous surface layer containing Fe^{3+} ($S=1/2$) allowed a more homogeneous distribution of Li and Li vacancies upon delithiation than the crystal with Fe^{2+} ($S=2$) state. Thus, it will partially contribute to improved properties for $LiFePO_4$/C. An analogous effect can be considered in our AH-$LiFePO_4$ sample, in which $LiFePO_4$ is also in close contact with the carbon filament matrix. The above observations indicate that the AH-$LiFePO_4$ particles are not only well inter-connected *via* $LiFePO_4$ —carbon shell—carbon network interactions but also that the void space in the carbon network might accommodate the electrolyte, leading to an intimate contact between $LiFePO_4$/C and electrolyte. Hence there is the potential for high rate capabilities whereby significant Li^+ ions can be transferred within a short period of time. Conversely, TEM observations (Fig. 3e and f) suggested that no such carbon filament matrix formed for A-$LiFePO_4$ and N-$LiFePO_4$ samples to accompany the shell coating which has been observed in composites previously.

The electrochemical properties of the $LiFePO_4$/C composites were evaluated by galvanostatic charge–discharge cycling using CR2032 coin cells. Fig. 4 presents the charge (Li extraction)–discharge (Li insertion) profiles of $LiFePO_4$/C electrodes at 1 C rate (1 C rate corresponds to 170 mA g^{-1}). All samples exhibited a flat discharge plateau at 3.4 V and a charge plateau at 3.5 V, which could be attributed to the $FePO_4/LiFePO_4$ redox reaction associated with the Li^+ ion extraction (charge) and Li^+ ion insertion (discharge) process. AH-$LiFePO_4$ samples yield the highest discharge capacity of 140 mA h g^{-1} at 1 C. By contrast, the N-$LiFePO_4$ sample, delivering the lowest capacity of 130 mA h g^{-1}, exhibited a retarded discharge behavior between 3.4–2.5 V versus Li^+/Li, (cf. the smooth discharge characteristics for the AH-$LiFePO_4$ in the same voltage range). This part of the discharge profile (3.4–2.5 V) was previously reported by Wu et al. as an interfacial Li storage process and is closely correlated with the nature of the interface between the active $LiFePO_4$ itself and the additive conductive carbon [32]. The conductive carbon matrix not only acts as an electrolyte container, but also serves as an elastic buffer to relieve the strain during Li insertion/extraction. One might therefore speculate that the interface between the spherical $LiFePO_4$/C particles and the 3D carbon network of the AH-$LiFePO_4$ could be responsible for the advantageous discharge behavior from 3.4 to 2.5 V, compared to N-$LiFePO_4$. The difference in morphology might also explain the high columbic efficiency of 99.2% for AH-$LiFePO_4$ compared to 96.2% for A-$LiFePO_4$ and 94.0% for N-$LiFePO_4$, during the 1st charge–discharge cycles.

Fig. 5 compares the cycling abilities of the prepared $LiFePO_4$/C composites at a 1 C rate. It was found that the AH-$LiFePO_4$ sample has the best cycling performance, with a retention of 98.8% of its initial capacity (123.7 mA h g^{-1}) after 50 cycles. The N-$LiFePO_4$ sample exhibits 90.5% of its initial capacity (95.2 mA h g^{-1}). Fig. 6 summarizes the high rate capabilities of the samples. Each cell was cycled for 20 cycles at a 1 C rate prior to the high rate test. The cells using AH-LiFePO4, A-LiFePO4 and N-$LiFePO_4$ were discharged at varied current rates: 1 C, 2 C, 5 C and 10 C, noting that the maximum original cell capacities could be recovered during a re-charge at 0.2 C rate. Accordingly, AH-$LiFePO_4$ demonstrated the best high rate performance, delivering capacities of 140, 123, 112 and 93 mA h g^{-1} at 1 C, 2 C, 5 C and 10 C rates respectively. Corresponding capacities for N-$LiFePO_4$ were only 130, 80, 52 and 37 mA h g−1. Hence the AH-$LiFePO_4$ is more tolerant to high current densities. For AH-$LiFePO_4$, the 3D carbon component serves two

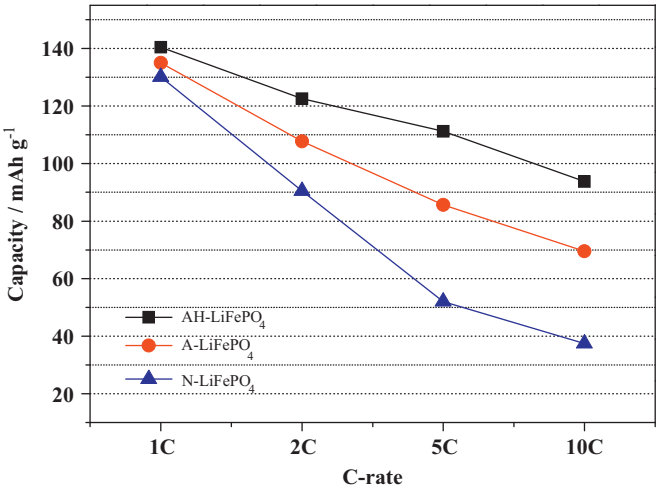

Fig. 6. Comparison of capacities obtained at various discharge rates for AH-$LiFePO_4$, A-$LiFePO_4$ and N-$LiFePO_4$ composites, following 20 cycles at 2 C.

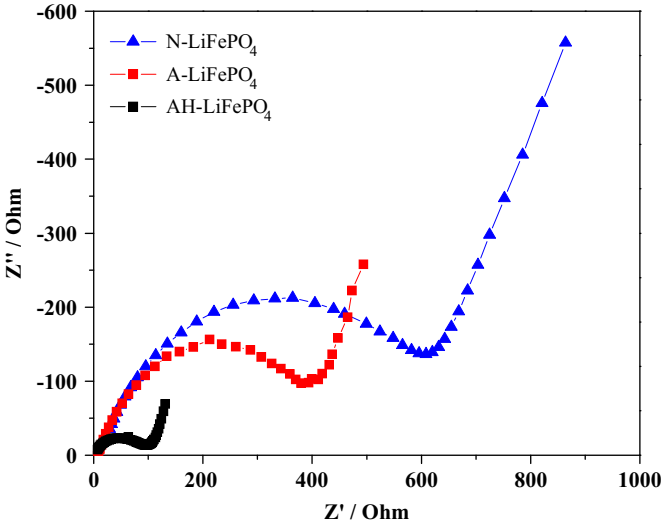

Fig. 7. Electrochemical impedance spectra for AH-$LiFePO_4$, A-$LiFePO_4$ and N-$LiFePO_4$ after 30 cycles.

functions: first as a mixed conducting 3D matrix and second as a conduct to facilitate access of the electrolyte to the electrode and is thus desirable for materials running at high current densities [33].

The effect of varying the carbon morphologies in $LiFePO_4$/C composites can also be determined by electrochemical impedance spectroscopy (EIS). Fig. 7 presents the EIS spectra of the samples after 30 charge–discharge cycles at a 2 C rate. The width of the semicircle at a relatively high frequency (corresponding to the charge transfer resistance) is much smaller for AH-$LiFePO_4$ than that for either of the other two composites, which indicates that the charge transfer resistance of the AH-$LiFePO_4$ nanocomposite is smaller than that of A-$LiFePO_4$ or N-$LiFePO_4$. This might be ascribed to an enhanced conductivity induced by the filament carbon matrix. The cyclic

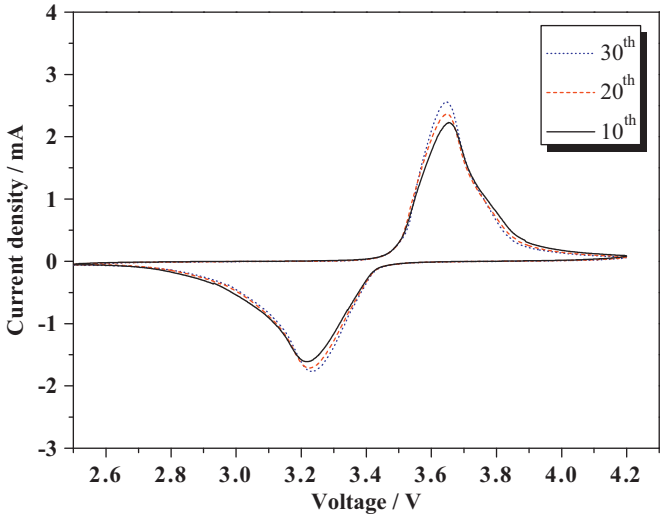

Fig. 8. CV curves for AH-$LiFePO_4$ at 10th, 20th and 30th cycles respectively at 0.3 mVs^{-1}.

voltammogram (CV) for AH-$LiFePO_4$ is shown in Fig. 8. The obtained plots exhibited highly symmetrical current peaks at 3.3 V and 3.6 V, corresponding to the Fe^{3+}/Fe^{2+} redox couple. The CV curves overlap closely, indicating high electronic conductivities. This observation is in good agreement with the results of EIS, and could also explain the high columbic efficiency observed for AH-$LiFePO_4$.

4. Conclusions

$LiFePO_4$/C composites were fabricated *via* a low-cost solid-state reaction from Fe and $FePO_4$ (as Fe sources) and Li_3PO_4 (as a Li source). A carbon network composed of filament-like carbon materials can be formed in-situ in $LiFePO_4$/C composites made with sucrose as a carbon source in a condition of partially reductive atmosphere and iron as catalyst. The form and morphologies of the carbon in the composites greatly affects the cycling and high rate performance. The resultant $LiFePO_4$/C composite has excellent high rate capabilities which could be attributable to anticipated 3D-conduction and excellent access to the electrolyte in the carbon matrix.

Acknowledgments

This work was supported by the International Science and Technology Cooperation Program of China (2012DFG42100), and the Doctoral Program of Higher Education of China (2011010113003), Zhejiang Provincial Natural Science Foundation of China (Grant no. LQ12B01003), Zhejiang University of Technology start-up fund (Grant no. 101009529), National Natural Science Foundation of China (NSFC, Grant nos. 20506024 and 21173190) and the State Key Development Program for Basic Research of china (Grant no. 2007CB216409).

References

[1] S. Luo, Z. Tang, J. Lu, Z. Zhang, Electrochemical properties of carbon-mixed $LiFePO_4$ cathode material synthesized by the ceramic granulation method, Ceramics International 34 (5) (2008) 1349–1351.

[2] T. Yuan, R. Cai, K. Wang, R. Ran, S. Liu, Z. Shao, Combustion synthesis of high-performance $Li_4Ti_5O_{12}$ for secondary Li-ion battery, Ceramics International 35 (5) (2009) 1757–1768.

[3] L. Wang, Y. Huang, R. Jiang, D. Jia, Preparation and characterization of nano-sized $LiFePO_4$ by low heating solid-state coordination method and microwave heating, Electrochimica Acta 52 (24) (2007) 6778–6783.

[4] J. Yao, C. Shen, P. Zhang, D.H. Gregory, L. Wang, Enhanced cycle ability of spinel $LiMn_2O_4$ by controlling the phase purity and structural strain, Journal of Physics and Chemistry of Solids 73 (11) (2012) 1390–1395.

[5] A. Kuwahara, S. Suzuki, M. Miyayama, High-rate properties of $LiFePO_4$/carbon composites as cathode materials for lithium-ion batteries, Ceramics International 34 (4) (2008) 863–866.

[6] C. Zhang, X. Huang, Y. Yin, J. Dai, Z. Zhu, Hydrothermal synthesis of monodispersed $LiFePO_4$ cathode materials in alcohol–water mixed solutions, Ceramics International 35 (7) (2009) 2979–2982.

[7] K.F. Hsu, S.Y. Tsay, B.J. Hwang, Synthesis and characterization of nano-sized $LiFePO_4$ cathode materials prepared by a citric acid-based sol–gel route, Journal of Materials Chemistry 14 (17) (2004) 2690–2695.

[8] W.-D. Yang, C.-Y. Hsieh, H.-J. Chuang, Y.-S. Chen, Preparation and characterization of nanometric-sized $LiCoO_2$ cathode materials for lithium batteries by a novel sol–gel method, Ceramics International 36 (1) (2010) 135–140.

[9] M. Higuchi, K. Katayama, Y. Azuma, M. Yukawa, M. Suhara, Synthesis of $LiFePO_4$ cathode material by microwave processing, Journal of Power Sources 119 (2003) 258–261.

[10] K. Hirose, T. Honma, Y. Benino, T. Komatsu, Glass–ceramics with $LiFePO_4$ crystals and crystal line patterning in glass by YAG laser irradiation, Solid State Ionics 178 (11–12) (2007) 801–807.

[11] K.S. Park, K.T. Kang, S.B. Lee, G.Y. Kim, Y.J. Park, H.G. Kim, Synthesis of $LiFePO_4$ with fine particle by co-precipitation method, Materials Research Bulletin 39 (12) (2004) 1803–1810.

[12] J. Yao, X. Wu, P. Zhang, S. Wei, L. Wang, Effects of Li_2CO_3 as a secondary lithium source on the LiFePO4/C composites prepared via solid-state method, Journal of Physics and Chemistry of Solids 73 (7) (2012) 803–807.

[13] Y.F. Wang, D. Zhang, X. Yu, R. Cai, Z.P. Shao, X.Z. Liao, Z.F. Ma, Mechanoactivation-assisted synthesis and electrochemical characterization of manganese lightly doped LiFePO(4), Journal of Alloys and Compounds 492 (1–2) (2010) 675–680.

[14] A.V. Murugan, T. Muraliganth, A. Manthiram, Rapid microwave-solvothermal synthesis of phospho-olivine nanorods and their coating with a mixed conducting polymer for lithium ion batteries, Electrochemistry Communications 10 (6) (2008) 903–906.

[15] A.K. Padhi, K.S. Nanjundaswamy, J.B. Goodenough, Phospho-olivines as positive-electrode materials for rechargeable lithium batteries, Journal of the Electrochemical Society 144 (4) (1997) 1188–1194.

[16] J.H. Park, J.S. Kim, E.G. Shim, K.W. Park, Y.T. Hong, Y.S. Lee, S.Y. Lee, Polyimide gel polymer electrolyte-nanoencapsulated LiCoO(2) cathode materials for high-voltage Li-ion batteries, Electrochemistry Communications 12 (8) (2010) 1099–1102.

[17] G.X. Wang, L. Yang, S.L. Bewlay, Y. Chen, H.K. Liu, J.H. Ahn, Electrochemical properties of carbon coated $LiFePO_4$ cathode materials, Journal of Power Sources 146 (1–2) (2005) 521–524.

[18] M.M. Doeff, J.D. Wilcox, R. Yu, A. Aumentado, M. Marcinek, R. Kostecki, Impact of carbon structure and morphology on the electrochemical performance of $LiFePO_4$/C composites, Journal of Solid State Electrochemistry 12 (7–8) (2008) 995–1001.

[19] F.F. Pan, W.L. Wang, H.J. Li, X.D. Xin, Q.Q. Chang, W.S. Yan, D.M. Chen, Investigation on a core–shell nano-structural LiFePO(4)/C and its interfacial C–O interaction, Electrochimica Acta 56 (20) (2011) 6940–6944.

[20] T.W. Ebbesen, H. Hiura, J. Fujita, Y. Ochiai, S. Matsui, K. Tanigaki, Patterns in the bulk growth of carbon nanotubes, Chemical Physics Letters 209 (1–2) (1993) 83–90.

[21] C.M. Burba, R. Frech, Raman and FTIR spectroscopic study of Li_xFePO_4 $(0<=x<=1)$, J Electrochem Soc 151 (7) (2004) A1032–A1038.

[22] K. Wang, R. Cai, T. Yuan, X. Yu, R. Ran, Z.P. Shao, Process investigation, electrochemical characterization and optimization of LiFePO(4)/C composite from mechanical activation using sucrose as carbon source, Electrochimica Acta 54 (10) (2009) 2861–2868.

[23] Y. Lin, M.X. Gao, D. Zhu, Y.F. Liu, H.G. Pan, Effects of carbon coating and iron phosphides on the electrochemical properties of $LiFePO_4$/C, Journal of Power Sources 184 (2) (2008) 444–448.

[24] Z.R. Chang, H.J. Lv, H.W. Tang, H.J. Li, X.Z. Yuan, H.J. Wang, Synthesis and characterization of high-density LiFePO(4)/C composites as cathode materials for lithium-ion batteries, Electrochimica Acta 54 (20) (2009) 4595–4599.

[25] F. Cheng, K.L. Huang, S.Q. Liu, J.L. Liu, R.J. Deng, Surfactant carbonization to synthesize pseudocubic alpha-Fe(2)O(3)/C nanocomposite and its electrochemical performance in lithium-ion batteries, Electrochimica Acta 56 (16) (2011) 5593–5598.

[26] J.R. Ying, C.R. Wan, C.Y. Jiang, Y.X. Li, Preparation and characterization of high-density spherical LiNi0.8Co0.2O2 cathode material for lithium secondary batteries, Journal of Power Sources 99 (1–2) (2001) 78–84.

[27] J. Zhao, J. He, J. Zhou, Y. Guo, T. Wang, S. Wu, X. Ding, R. Huang, H. Xue, Facile synthesis for $LiFePO_4$ nanospheres in tridimensional porous carbon framework for lithium ion batteries, Journal of Physical Chemistry C 115 (6) (2011) 2888–2894.

[28] J.M. Chen, C.H. Hsu, Y.R. Lin, M.H. Hsiao, G.T.K. Fey, High-power LiFePO4 cathode materials with a continuous nano carbon network for lithium-ion batteries, Journal of Power Sources 184 (2) (2008) 498–502.

[29] G.X. Wang, B. Wang, X.L. Wang, J. Park, S.X. Dou, H. Ahn, K. Kim, Sn/graphene nanocomposite with 3D architecture for enhanced reversible lithium storage in lithium ion batteries, Journal of Materials Chemistry 19 (44) (2009) 8378–8384.

[30] P.E. Nolan, M.J. Schabel, D.C. Lynch, A.H. Cutler, Hydrogen control of carbon deposit morphology, Carbon 33 (1) (1995) 79–85.

[31] K. Zaghib, A. Mauger, F. Gendron, C.M. Julien, Surface effects on the physical and electrochemical properties of thin $LiFePO_4$ particles, Chemistry of Materials 20 (2) (2008) 462–469.

[32] X.L. Wu, L.Y. Jiang, F.F. Cao, Y.G. Guo, L.J. Wan, LiFePO(4) nanoparticles embedded in a nanoporous carbon matrix: superior cathode material for electrochemical energy-storage devices, Advanced Materials 21 (25–26) (2009) 2710–2715.

[33] M. Yang, Q. Gao, $LiFePO_4$/C composite cathode material with a continuous porous carbon network for high power lithium-ion battery, Journal of Alloys and Compounds 509 (8) (2011) 3690–3698.